AGU PUBLICATIONS

JGR

Journal of Geophysical Research: Atmospheres

RESEARCH ARTICLE
10.1002/2016JD025344

Key Points:
- In situ and spaceborne observations of the Kelud plume
- Persistence of ash in the lower stratosphere
- Ash can impact climate on longer time scale than previously thought

Correspondence to:
J.-P. Vernier,
jeanpaul.vernier@nasa.gov

Citation:
Vernier, J.-P., T. D. Fairlie, T. Deshler, M. Natarajan, T. Knepp, K. Foster, F. G. Wienhold, K. M. Bedka, L. Thomason, and C. Trepte (2016), In situ and space-based observations of the Kelud volcanic plume: The persistence of ash in the lower stratosphere, *J. Geophys. Res. Atmos.*, *121*, 11,104–11,118, doi:10.1002/2016JD025344.

Received 10 MAY 2016
Accepted 1 SEP 2016
Accepted article online 4 SEP 2016
Published online 24 SEP 2016

In situ and space-based observations of the Kelud volcanic plume: The persistence of ash in the lower stratosphere

Jean-Paul Vernier[1,2], T. Duncan Fairlie[2], Terry Deshler[3], Murali Natarajan[2], Travis Knepp[1,2], Katie Foster[3], Frank G. Wienhold[4], Kristopher M. Bedka[2], Larry Thomason[2], and Charles Trepte[2]

[1]Science Systems and Applications, Inc., Hampton, USA, [2]NASA Langley Research Center, Hampton, Virginia, USA, [3]Department of Atmospheric Science, University of Wyoming, Laramie, Wyoming, USA, [4]Swiss Federal Institute of Technology (ETHZ), Zurich, Switzerland

Abstract Volcanic eruptions are important causes of natural variability in the climate system at all time scales. Assessments of the climate impact of volcanic eruptions by climate models almost universally assume that sulfate aerosol is the only radiatively active volcanic material. We report satellite observations from the Cloud-Aerosol Lidar with Orthogonal Polarization (CALIOP) on board the Cloud-Aerosol Lidar and Infrared Pathfinder Satellite Observations (CALIPSO) satellite after the eruption of Mount Kelud (Indonesia) on 13 February 2014 of volcanic materials in the lower stratosphere. Using these observations along with in situ measurements with the Compact Optical Backscatter AerosoL Detector (COBALD) backscatter sondes and optical particle counters (OPCs) made during a balloon field campaign in northern Australia, we find that fine ash particles with a radius below 0.3 μm likely represented between 20 and 28% of the total volcanic cloud aerosol optical depth 3 months after the eruption. A separation of 1.5–2 km between the ash and sulfate plumes is observed in the CALIOP extinction profiles as well as in the aerosol number concentration measurements of the OPC after 3 months. The settling velocity of fine ash with a radius of 0.3 μm in the tropical lower stratosphere is reduced by 50% due to the upward motion of the Brewer-Dobson circulation resulting a doubling of its lifetime. Three months after the eruption, we find a mean tropical clear-sky radiative forcing at the top of the atmosphere from the Kelud plume near $-0.08\ W/m^2$ after including the presence of ash; a value ~20% higher than if sulfate alone is considered. Thus, surface cooling following volcanic eruptions could be affected by the persistence of ash and should be considered in climate simulations.

1. Introduction

Global-mean surface and tropospheric temperatures have remained relatively unchanged between 1995 and 2010, despite a 0.4–0.5°C warming predicted by the climate models used for the last Climate Model Initiative Project 5 (CMIP5) (Intergovernmental Panel on Climate Change AR5). Among the reasons evoked to explain this discrepancy are the cooling impacts of several volcanic eruptions.

Over the past 15 years, several moderate volcanic eruptions observed by satellites [*Vernier et al.*, 2011; *Santer et al.*, 2014; *Andersson et al.*, 2015] have significantly mitigated the global warming which would have otherwise occurred [*Solomon et al.*, 2011; *Fyfe et al.*, 2013]. Large volcanic events like Mount Pinatubo's 1991 eruption are known to affect our climate system through the radiative impact of the sulfate aerosol layer produced from the oxidation of SO_2 and homogenous nucleation of H_2SO_4 and water [*Hamill et al.*, 1997]. Sulfate aerosols efficiently scatter solar radiation back into space and absorb upcoming long-wave terrestrial radiation leading to surface temperature cooling and stratospheric warming [*Robock*, 2000]. In most climate models, volcanic aerosols are assumed to be entirely sulfate; the result of the oxidation of SO_2 and condensation of the resultant sulfuric acid. Radiative calculations based on assuming purely sulfate lead to an average radiative forcing, at the top of the atmosphere, near $-25\ Wm^{-2}$ per unit of aerosol optical depth (AOD) [*Hansen et al.*, 1992, 2005]. This conversion factor, which is commonly used to convert AOD retrieved by space-based instruments into volcanic radiative forcing [e.g., *Solomon et al.*, 2011], ignores any impacts due to ash.

After a volcanic eruption, ash particles are assumed to be rapidly removed through wet scavenging and dry sedimentation [*Niemeier et al.*, 2009] and are thus not considered to have a significant impact on climate. In this study, we investigate the optical properties and composition of the volcanic plume following the

Keluderuption on 13 February 2014 using spaceborne observations as well as in situ measurements. These measurements confirm the persistence of ash in the Kelud volcanic plume 3 months after the eruption.

The paper is constructed as follows: In section 2, we describe the retrievals used to separate ash and sulfate components in the Cloud-Aerosol Lidar and Infrared Pathfinder Satellite Observations (CALIPSO) satellite data and the in situ observations of the Kelud plume made during a balloon field campaign in May 2014. Section 3 shows the resulting profiles of ash and sulfate optical properties from CALIPSO during the first 90 days after the Kelud eruption, while the in situ data are shown in section 4. We use satellite and in situ data to constrain radiative calculations in sections 5 and 6. Finally, in section 7, we discuss the implications of accounting for ash in climate simulations.

2. Data Sets and Methods

2.1. CALIPSO

The Cloud-Aerosol Lidar with Orthogonal Polarization (CALIOP) lidar on board the CALIPSO satellite makes range-resolved measurements of elastic backscatter at 532 nm and 1064 nm and of linear depolarization ratio (the ratio between perpendicular and parallel backscatter) at 532 nm [*Winker et al*., 2010]. After years of nearly continuous observations, studies of several volcanic plumes in the upper troposphere/lower stratosphere region have shown that depolarization and color ratios (the ratio between 1064 and 532 nm backscatter) provide information about particle shape and size, which is useful to distinguish volcanic ash, sulfate aerosol layers, and ice clouds [*Hayashida et al*., 1984; *Winker and Osborn*, 1992; *Winker et al*., 2012; *Vernier et al*., 2009, 2013]. We use CALIOP depolarization measurements, which are sensitive to particle sphericity, to separate the contribution of spherical sulfate aerosol and irregular ash particles to the total backscatter.

CALIOP makes measurements at 532 nm of total attenuated backscatter, β_t, perpendicular and parallel backscatter, $\beta_\perp$, and $\beta_{//}$ from which volume depolarization ratio, ∂, particulate backscatter, β_p, and scattering ratio, SR, can be derived according to equations (1)–(3). Molecular backscatter, β_m, is computed from air density obtained from the Goddard Earth Observing System model version 5. The CALIPSO measurements are corrected for Rayleigh scattering and ozone absorption but not for Mie scattering. The lidar signal attenuation from stratospheric aerosol above the Kelud volcanic plume is expected to affect the transmission by less than 2% and is not corrected here.

$$\partial = \beta_\perp/\beta_{//} = \beta_\perp/(\beta_t - \beta_\perp) \tag{1}$$

$$\beta_p = \beta_t - \beta_m \tag{2}$$

$$SR = \beta_t/\beta_m \tag{3}$$

The ash and sulfate backscatter fractions can be derived following *Sugimoto and Lee*, [2006], *Tesche et al.* [2009], and *Ansmann et al.* [2011]. First, the particulate depolarization ratio ∂_p is calculated from ∂ and SR following *Cairo et al.* [1999], according to equation (4) with $\partial_m = 0.0037$.

$$\partial_p = \frac{\mathrm{SR}\times\partial\times(\partial_m+1) - \partial_m\times(\partial+1)}{\mathrm{SR}\times(\partial_m+1) - (\mathrm{SR}+1)} \tag{4}$$

Given (∂_p) and the theoretical ash ($\partial_a = 0.36+/-0.02$) and sulfate depolarization ratios ($\partial_s = 0.01+/-0.01$) [*Ansmann et al*., 2011], the ash-related attenuated backscatter, β_a, sulfate-related attenuated backscatter coefficients, β_s, and ash backscatter fraction, *F*, can be written as

$$\beta_a = \beta_p \frac{(\partial_p - \partial_s)(1+\partial_a)}{(\partial_a - \partial_s)(1+\partial_p)} \tag{5}$$

$$\beta_s = \beta_p - \beta_a \tag{6}$$

$$F(\%) = 100\times\left(\beta_a/\beta_p\right) \tag{7}$$

We use equations (5)–(7) to separate the contributions of ash and sulfate backscatter from the total backscatter coefficient as measured by CALIOP. We then derive extinction coefficients for aspherical ash particles, α_a, and liquid sulfate aerosol, α_s, assuming lidar ratios (extinction-to-backscatter ratios) of $L_s = 40$ *sr*(±10 sr) [*Jager and Deshler*, 2002, 2003; *Mattis et al*., 2010] and $L_s = 50$ *sr* (±10 sr) [*Ansmann et al*., 2011] for sulfate and ash,

respectively. The 20–25% uncertainty in the lidar ratios for ash and sulfate leads to a 20–25% uncertainty in the total ash and sulfate AOD for the Kelud plume.

$$\alpha_s = \beta_s \cdot L_s \tag{8}$$

$$\alpha_a = \beta_a \cdot L_a \tag{9}$$

2.2. Method Limitation and Error Analysis

The method used to separate the contributions of ash and sulfate to the total backscatter assumes that ash and sulfate are externally mixed so that the particulate depolarization ratio is linearly related to known ash and sulfate depolarization ratios. *Schumann et al.* [2011] argued that coated particles can retain their asphericity, based on observations made during several field campaigns dedicated to the study of mineral dusts. Ash particles coated with sulfuric acid have been observed from the NASA DC-8 aircraft using scanning electron microscopy after the Mount Pinatubo eruption [*Pueschel et al.*, 1994] demonstrating that internally mixed volcanic aerosols exist. These aspherical particles were found at the bottom of the Mount Pinatubo plume with geometric radius of ~0.8 μm, in contrast with sulfate aerosol observed from the ER-2 aircraft near 20 km with a radius of ~0.4 μm [*Pueschel et al.*, 1994]. Higher lidar depolarization values were observed near the bottom of the Pinatubo plume [*Browell et al.*, 1993] confirming the presence of larger, aspherical particles at lower altitudes.

We follow *Ansmann et al.* [2011] in choosing an ash particulate depolarization ratio of 0.36. This value is given with an uncertainty of ±0.02 and was derived from ground-based lidar depolarization measurements over Munich and Leipzig during the plume transport episode following the 2010 Eyjafjallajökull eruption [*Ansmann et al.*, 2010; *Groß et al.*, 2010]. This value is also supported by CALIOP observations of the Puyehue Cordon plume, which showed a depolarization ratio probability density function centered near 0.35 during the first 30 days after this eruption (Figure 11). The Puyehue-Cordon eruption was associated with an extremely small amount of injected SO_2 so that the plume is consistent with ash without sulfate aerosol.

Assuming an uncertainty of near 10% on the ash depolarization ratio (±0.04) leads to an uncertainty of 8% on the retrieved ash AOD between 18 and 23 km. A 10% uncertainty on the theoretical sulfate depolarization ratio leads to uncertainty on the retrieved ash and sulfate AOD of less than 10%. Uncertainties associated with the CALIOP lidar calibration (5%), model density (3%), lidar ratios (25%), and depolarization ratios (10%) yield an overall uncertainty on the sulfate and ash AODs near 30%.

For our study, internally mixed ash and sulfate would lower the mean volume depolarization and consequently underestimate the ash contribution to backscatter and extinction. Given the lack of in situ particle measurements, it is very difficult to quantity the potential effect on our calculations.

2.3. In Situ Observations of the Kelud Plume

We conducted the KlAsh (Kelud-ash) field campaign in northern Australia 14–24 May 2014 to make aerosol profile measurements using balloon-borne in situ instruments. Aerosol backscatter was measured on five occasions using the Compact Optical Backscatter AerosoL Detector (COBALD). Aerosol size distribution and volatility was measured once. All measurements were flown within the Kelud plume from near Darwin, Australia (12.4°S, 130.8°E). COBALD is a light-weight (540 g) backscatter instrument, suitable for small balloon soundings [*Brabec et al.*, 2012]. Two high-power LEDs emit about 250 mW optical power at wavelengths of 455 nm and 940 nm. The light scattered back to the instrument from molecules, aerosols, and cloud particles is recorded by a silicon photodiode using phase sensitive detection.

The optical particle counter (OPC) flown by the University of Wyoming [*Deshler et al.*, 2003] provides vertical profiles of size-resolved aerosol concentration at 8 radii between 0.075 and 15 μm. For the Darwin flight a second OPC with an inlet heated to 180°C was included to determine the nonvolatile fraction of aerosol concentration. In addition, a condensation nuclei (CN) counter was added to the OPCs to measure the total aerosol number concentration [*Campbell and Deshler*, 2014].

3. CALIPSO Observations of the Kelud Volcanic Plume

On 13 February 2014, the Kelud volcano, located near 4°S on the island of Java (Indonesia), erupted for a few hours, injecting material deep into the tropical stratosphere. Kelud (also known as Kelut) is a stratovolcano with a summit elevation near 1731 m above sea level. Kelud is considered as one of the most dangerous volcanoes in

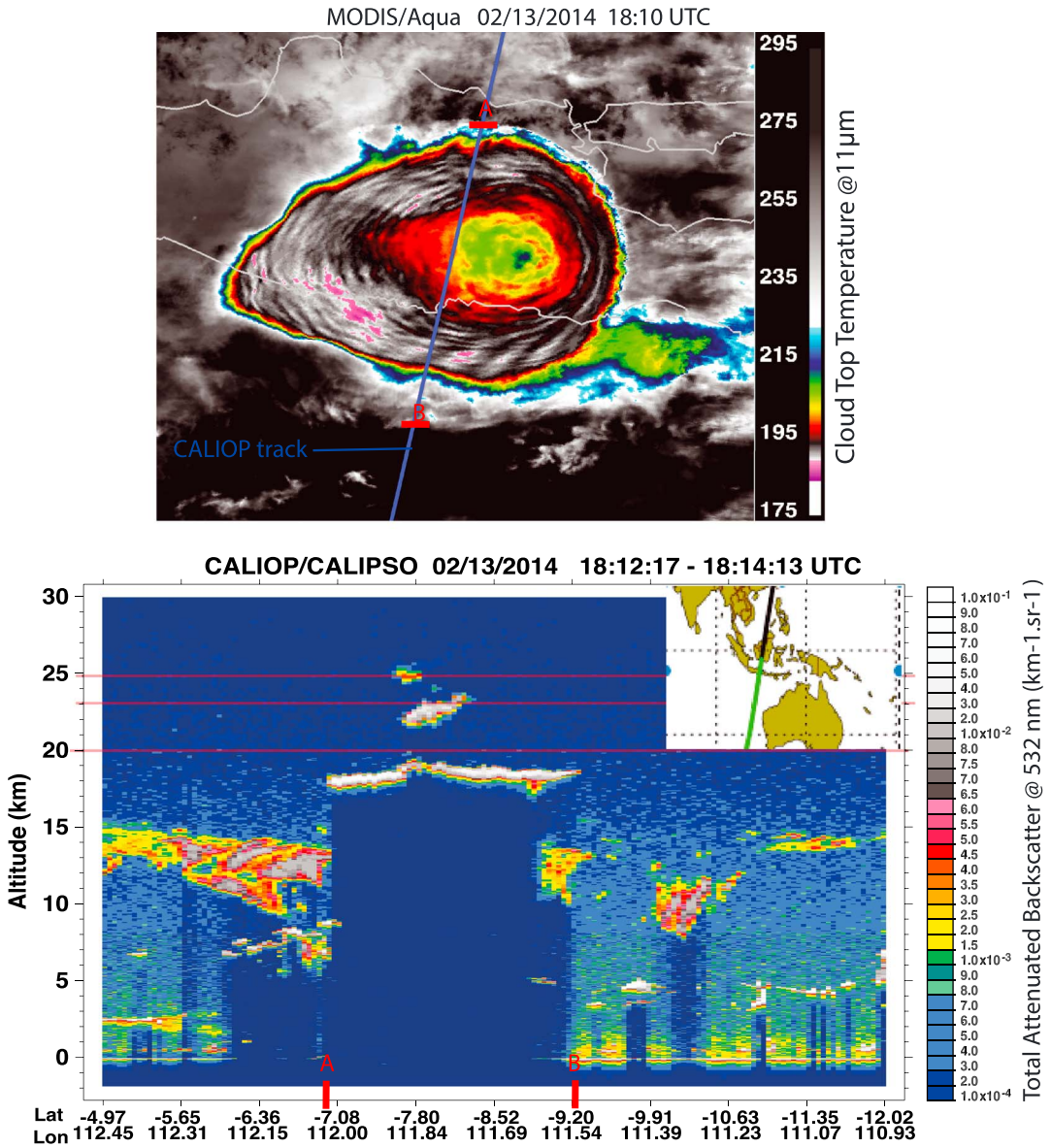

Figure 1. (top) Brightness temperature (11 µm) from MODIS/Aqua together with (bottom) the CALIOP/CALIPSO total attenuated backscatter lidar profiles along the orbit track. The Kelud volcanic cloud is seen through a large area of BT below 200 K with a warm region at the center indicative of deep stratospheric intrusions. CALIPSO shows that the plume reached up to 26 km with a main cloud near 18–19 km.

Java because of its frequent eruptions, deadly lahars, pyroclastic flows, and surges and is responsible for the deaths of thousands of people since 1500°AD. Figure 1 shows a curtain of total attenuated backscatter from a CALIPSO overpass only 40 min after the eruption together with a map of cloud top brightness temperature (BT) around the volcano from the Moderate Resolution Imaging Spectroradiometer (MODIS) on Aqua at 11 µm. An area of BT near 215 K is surrounded by very cold anvil clouds at 190 K. Based on the nearest radio sounding in Indonesia (not shown), the warmest BT core of the volcanic cloud is consistent with a volcanic plume in equilibrium with air near 25 km, which is consistent with the CALIOP observations.

Using infrared emissions (infrared atmospheric sounding interferometer and Atmospheric Infrared Sounder) and the UV backscatter satellite-borne instruments of Ozone Monitoring Instrument (OMI), the total SO_2 injected was estimated to be near 0.1–0.2 Tg [*Kristiansen et al.*, 2015], half the amount injected by Soufriere Hills in May 2006 [*Carn and Prata*, 2010] and 10–20 times smaller than the Nabro burden in June 2011 [*Clarisse et al.*, 2014].

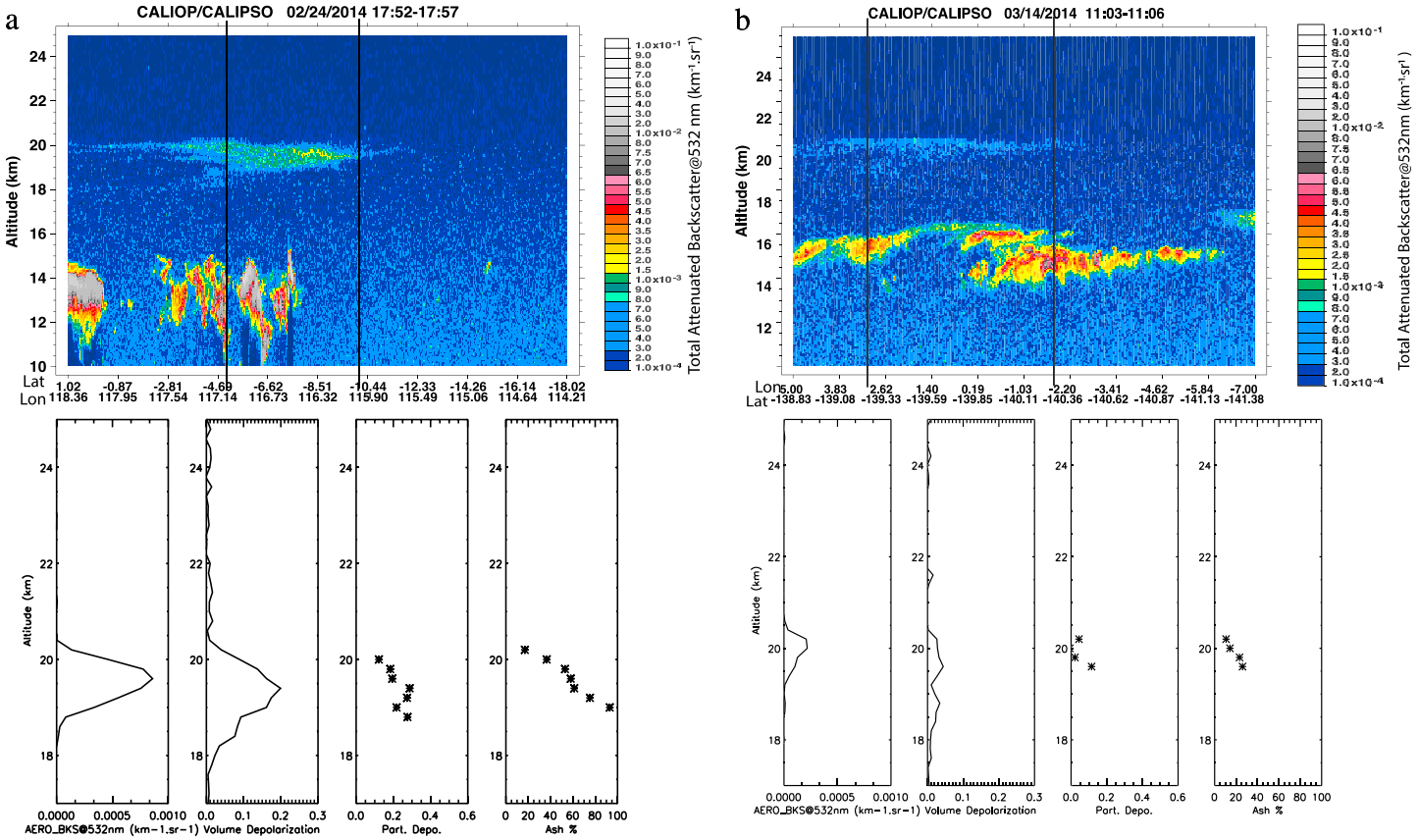

Figure 2. (a) CALIOP/CALIPSO total attenuated backscatter at 532 nm curtain from the 24 February 2014 at 1800 UTC orbit track. Mean profiles of aerosol attenuated backscatter, volume depolarization, particulate depolarization, all at 532 nm, and ash backscatter percentage averaged within 5 S–10 S. Note that particulate depolarization and ash fraction data are plotted for aerosol backscatter greater than 5.10^{-5} km^{-1} sr^{-1}. (b) Same as Figure 2a for the orbit track on 14 March 2014 at 1108 UTC. Profiles are averaged between 3°N and 2°S.

The CALIPSO curtain (Figure 1) confirms the presence of volcanic materials up to 26 km with the main volcanic cloud near 18–19 km. This is the highest level reached by a volcanic eruption since Mount Pinatubo in 1991. MODIS/Aqua and CALIOP/CALIPSO provided unprecedented, quasi-simultaneous observations of a volcanic cloud during the active phase of an eruption.

During the first few days after the eruption, the plume was observed along several CALIPSO orbit tracks. A curtain of total attenuated backscatter on 24 February 11 days after the eruption, over Indonesia (Figure 2a), shows the Kelud plume located near 19–21 km within the tropical stratosphere. Mean profiles of volume and particulate depolarization ratios (Figure 2a) suggest that the plume is largely composed of irregularly shaped particles. Since ice is expected to evaporate quickly, it is most likely that these observations indicate the presence of aspherical ash particles. We find a strong vertical gradient in ash backscatter fraction within the plume with nearly 20% of backscatter at the top and almost 100% at the bottom due to ash. These results suggest the sedimentation of larger ash particles at the bottom of the plume and the presence of recently formed small sulfate aerosol droplets at the level of the initial injection. We cannot completely rule out that the vertical separation of ash and sulfate could have occurred during the injection itself, but this is unlikely. Nearly a month after the eruption, on 14 March, the particulate depolarization has decreased below 0.2 and ash backscatter fraction remains near 20–30% at the bottom of the plume (Figure 2b).

Figure 3 shows the probability distribution functions (PDF) of the particulate depolarization ratio from 18 to 25 km and from 20°N to 20°S every 10 days during the first 3 months after the Kelud eruption. The PDF at 0–10 days of measurements captures a large ash fraction that has apparently quickly fallen out. After 10 days, the PDFs gradually shift with time toward lower depolarization values, consistent with

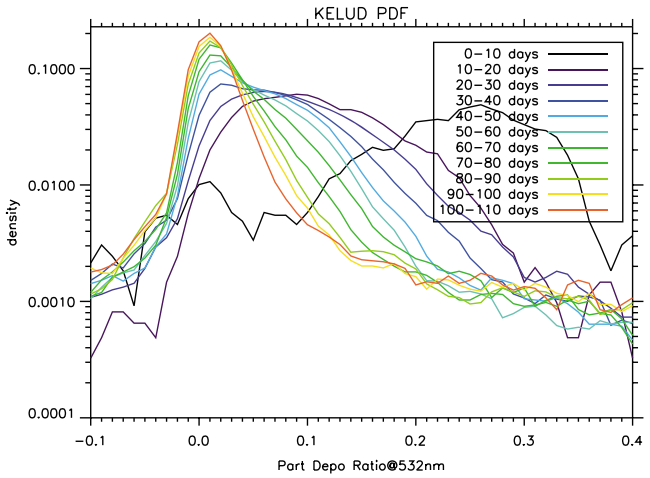

Figure 3. Probability density functions (PDF) of particulate depolarization calculated over 10 day periods between 20°N and 20°S and 18–25 km since the Kelud eruption. Note the shift of the PDFs toward low depolarization ratio values consistent with the removal of ash and formation of sulfate aerosol.

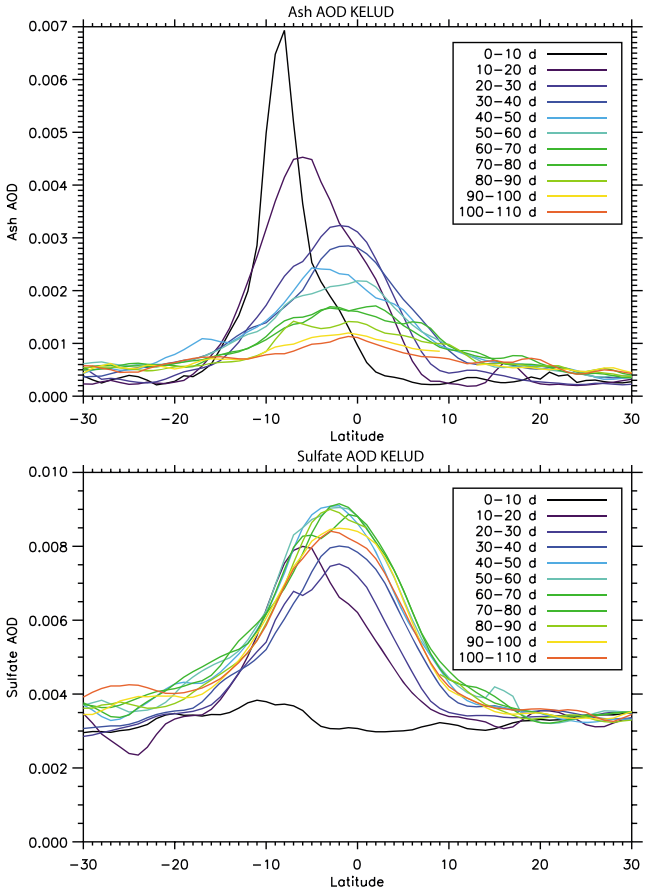

Figure 4. Ash and sulfate AODs at 532 nm calculated from CALIOP over 10 day periods between 20°N and 20°S and 18–25 km since the Kelud eruption.

the removal of ash particles and the progressive formation of sulfate and/or the coating of ash particles by sulfate aerosol, which would increase the apparent sphericity of aerosols within the plume. Compared to the PDF of the Soufriere Hills plume (not shown), we find that the Kelud PDF is skewed toward positive values suggesting the persistence of significant quantities of ash several months after the eruption.

We examine the evolution of the Kelud plume using latitudinal cross sections every 10 days of the mean aerosol optical depth (AOD) at 532 nm between 18 and 25 km for ash and sulfate, using the separation method described in section 1 (Figure 4). In addition, mean tropical (20°N–20°S) extinction profiles for ash and sulfate are also shown in Figure 5. During the first 10 days after the eruption, ash particles dominate the composition of the plume with a particle depolarization mode near 0.3 (Figure 3). The mean ash AOD peaks around 10°S with peaks at 18–19 km and a secondary peak at 23 km (Figure 4). Between 10 and 20 days, the plume is composed of nearly an equal mixture of sulfate and ash (Figure 5). The sulfate extinction profile shows a double structure with maxima at 18.5 and 20 km, suggesting that large but apparently spherical particles are present in the lowest part of the Kelud plume while small spherical aerosol remains higher up. This would be consistent with the coating of ash particles by sulfate aerosol, which would render ash particles larger and more spherical, thus subject to faster sedimentation. Alternatively, this feature could be explained by another mode of sulfate aerosol with larger radius.

The progressive changes in the optical properties of the plume (Figures 3–5) are consistent with the formation of sulfate aerosol from the oxidation of SO_2. Sulfate extinction coefficients and AOD values are shown to exceed

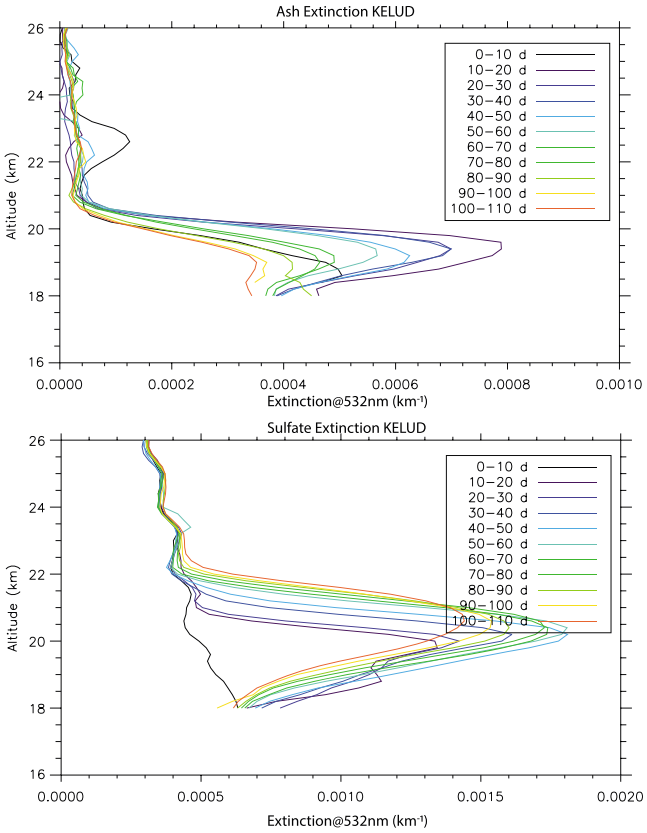

Figure 5. Averaged ash and sulfate extinction profiles calculated over 10 day periods between 20°N and 20°S since the Kelud eruption.

those of ash after 20 days, while no clear distinction in the location of the ash and sulfate clouds in latitude is visible (Figure 5). Nevertheless, a small but distinguishable difference of a few hundred meters in the altitude of the peaks in ash and sulfate extinction profiles suggests that ash particles, which are likely larger with higher density, are accumulating at the base of the plume, with smaller lighter sulfate aerosol remains above. The altitude separation of the plume composition becomes even more evident after 40–50 days (Figure 5) when the peaks in sulfate and ash are nearly 1 km apart. Finally, more than 3 months after the eruption, the ash and sulfate clouds are separated by ~1.5 km. We note also an increase in sulfate AOD in the Southern Hemisphere (15°S–30°S) from 0.003 to 0.004 within 3 months consistent with the wave-driven meridional transport of the Kelud plume by the lower branch of the Brewer Dobson circulation, which is particularly active during the western phase of the quasi-biennial oscillation [*Trepte and Hitchman*, 1992] as observed during the first half of 2014 (www.geo.fu-berlin.de/en/met/ag/strat/produkte/qbo/).

Overall, ash dominates the aerosol extinction profiles during the first 2 weeks after the Kelud eruption, while extinction due to sulfate aerosol increases progressively thereafter. Peaks in averaged ash extinction profiles (Figure 5) appear 1.5 km lower than the sulfate peaks after 90 days.

4. Balloon-Borne Measurements of the Kelud Plume

Three months after the eruption of Mount Kelud, we conducted the KlAsh balloon field campaign in Darwin, Australia, to further explore the composition of the Kelud plume. KlAsh combined light and heavy balloon payloads to profile the optical properties and size distribution of nonvolatile (ash) and volatile (sulfate) particles. Between 14 and 24 May 2014, five light-weight COBALD sondes were flown from the Bureau of Meteorology in Darwin (12.4°S, 130.9°E). On 20 May 2014, one large gondola containing two OPCs, one CN, and one COBALD was flown from Coroborree (12.7°S, 131.5°E). One of the OPCs had an inlet heated to 180°C, to constrain the measurements to nonvolatile particles.

During the campaign, we used trajectory mapping of aerosol scattering ratio obtained from CALIOP observations [*Vernier et al.*, 2013] to predict the position of the Kelud plume and to provide guidance for the balloon flights. While payload recovery, aviation authorization, and logistics were the dominant factors for flight planning, the forecast guidance strongly motivated us to start the campaign soon after our arrival in Australia. While the volcanic plume had stayed north of Darwin in the week leading up to our deployment, volcanic material was predicted over the coast of northern Australia on 17–18 May, providing favorable conditions to fly the COBALD sondes.

The location of the Kelud plume is illustrated in Figure 6 (top), which shows a map of CALIOP observations of the mean SR between 18 and 22 km accumulated between 14 and 24 May 2014. Elevated SR associated with

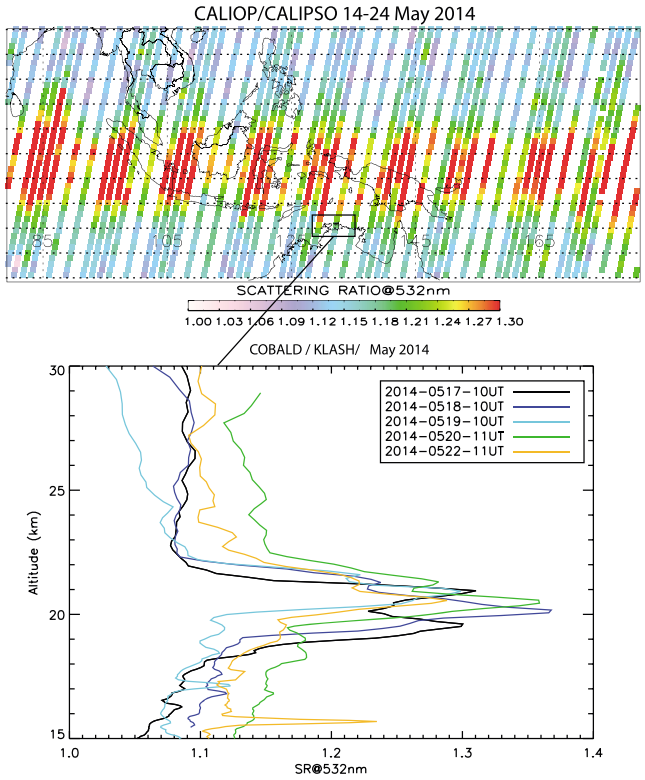

Figure 6. (top) Accumulated CALIOP measurements from 14 to 24 May 2014 of mean SR at 532 nm between 18 and 22 km. (bottom) High-resolution SR profiles from the COBALD flights at 532 nm obtained during KIAsh. The black box highlights the location of the balloon campaign.

the Kelud plume is mostly confined near the equator but also extends to the coast of northern Australia near 10°S. Figure 5 (bottom) shows the scattering ratio (SR) profiles at 532 nm derived from the five COBALD flights using a method described by *Vernier et al.* [2015]. Enhanced backscatter observed between 18.5 and 21.5 km on the first COBALD flight (17 May) corresponds to the Kelud plume, consistent with CALIOP observations (Figure 5, top). Notable features of this flight are the double peaks in SR of ~1.3 at 19 and 21 km. These features are consistent with CALIOP (Figure 4b), which show a vertical separation between ash and sulfate extinction profiles, and peaks near 19 and 20.5 km, respectively, similar to those observed by COBALD. The additional COBALD flights at Darwin (3 months after the eruption) show profiles with only modest enhancements of SR below 20 km. Given that CALIPSO showed Darwin to be at the very edge of the volcanic plume, this variability is almost certainly due to differences in horizontal advection and spatial gradients for upper and lower parts of the plume.

The potential vertical separation of sulfate and ash particles in the plume was a focus of the large OPC flight from Corroboree (12.7°S, 131.5°E) on 20 May. Figure 7 shows profiles of number concentration for total (black) and nonvolatile particles (red) for four size ranges. Nonvolatile particles dominate the population of aerosol of radius greater than 0.26 μm below 20 km. There is a clear altitude separation between the peaks in the nonvolatile and volatile aerosol populations. A small layer 19–21 km is observed on the nonvolatile aerosol concentration profiles for $r > 0.078$ μm, while the volatile layer extends above 22 km. For $r > 0.15$ μm, there is a hint of a nonvolatile particle layer 18–20 km and a clear volatile layer 20–22 km. Most of the particles for $r > 0.26$ μm and $r > 0.37$ μm consist of nonvolatile ash particles. While we cannot determine for certain that the initial injection heights of SO2 and ash are identical, larger particles are found at lower altitudes than are smaller particles as would be expected from sedimentation.

We use a simple 1-D model based upon Stokes' equation (equation (10)) to simulate the sedimentation of particles composing the Kelud plume where the terminal velocity, V_{TS}, is

$$V_{TS} = \frac{\rho d^2 g C_c}{18\eta} \tag{10}$$

where d and ρ are the diameter and mass density of the particles, g is the gravitational constant, η is the air dynamical viscosity ($\eta = 1.422 \times 10^{-5}$ N s/m^2 near 20 km), and C_c is the slip correction factor:

$$C_c = 1 + \frac{\lambda}{dp}\left[2.34 + 1.05\exp\left(-0.39\frac{dp}{\lambda}\right)\right] \tag{11}$$

where λ is the mean-free path. For air, $\lambda = 0.83$ μm for temperature and pressure near 20 km.

Table 1 shows the rate of settling of sulfate and ash particles of sizes corresponding to those measured during the OPC flight shown in Figure 7. Theoretical calculations (Table 1) suggest that sulfate particles of 0.08 μm

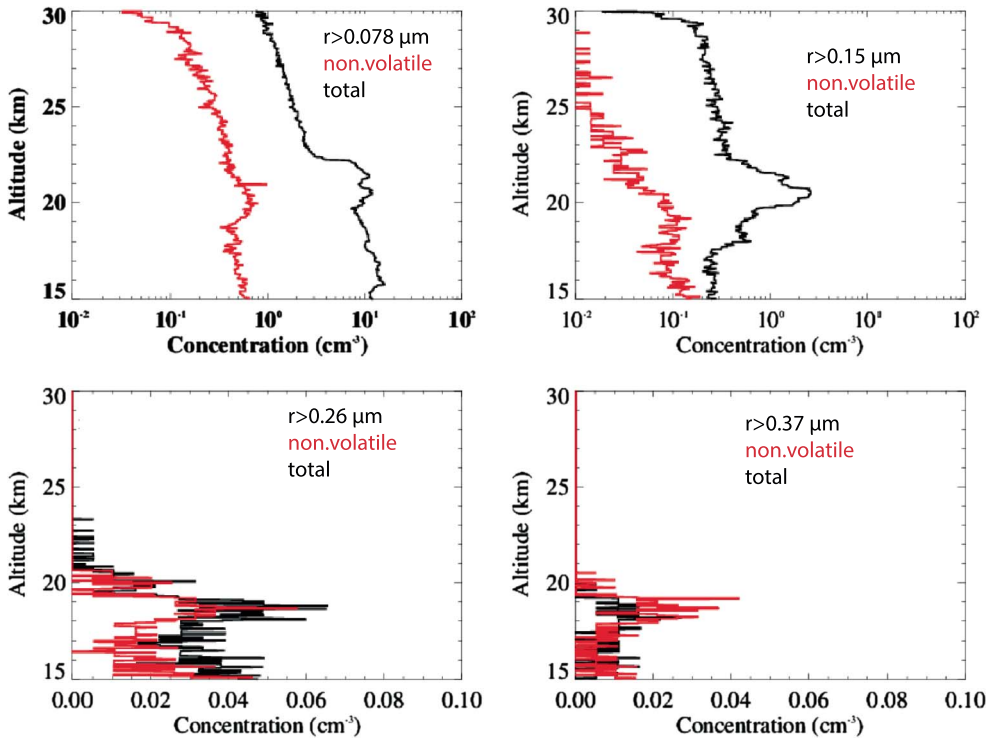

Figure 7. Profiles of total (black) and nonvolatile (red) particle number concentration obtained during a large balloon flight from Corroboree on 20 May 2014.

and 0.37 µm, using a mass density of 1670 kg/m^3 consistent with a mixture of 75% H_2SO_4 and 25% water, should be separated by around 1.0 km after 3 months.

Volcanic layers populated by particles with radius of 0.37 µm are seen on the OPC profiles near 17.5–19.5 km, while layers of 0.08 µm aerosol are located near 20–22 km. The 2.5 km plume separation is greater than predicted by the Stokes velocity.

The OPC measurements indicate that most of the particles with $r > 0.26$ µm composing the volcanic plume are nonvolatiles and most likely ash. Using a particle density of 2500 kg/m^3, generally assumed for ash [*Hobbs et al.*, 1991], the predicted separation between ash and sulfate becomes 1.6 km in better agreement with the observations. To achieve the separation observed would require a particle density near 3700 kg/m^3, assuming no additional vertical velocity of the air. Calculated and observed vertical separations between the ash and sulfate clouds are well within the uncertainties associated with particle radius adopted, assumed densities, vertical advection, and turbulence.

Air in the tropical lower stratosphere is subject to a diabatic ascent of nearly 300 m/month [*Rosenlof*, 1995; *Corti et al.*, 2005] associated with the upward branch of the Brewer-Dobson circulation. Volcanic sulfate with radius below 0.15 µm can be transported upward since its settling velocity is less than the upward motion of the BD circulation (for example, Soufriere Hills [*Vernier et al.*, 2009]). In addition, the sedimentation of fine ash particles can also be reduced allowing them to remain in the lower stratosphere for months. Ash particles with radius near 0.26 µm found in the Kelud plume would take nearly 17 months to descend 2 km in the

Table 1. Theoretical Calculation of Sedimentation Rate of Particles of 0.08, 0.15, 0.26, and 0.37 µm Radius, Using a Mass Density of 1670 kg/m^3 for Sulfate and 2500 kg/m^3 for Ash

Particle Radius (µm)	Slip Factor (No Unit)	Sedimentation Rate (m/Month)
0.08	30 (sulfate)	79 (sulfate)
0.15	16 (sulfate)	154 (sulfate)
0.26	10 (sulfate/ash)	279 (sulfate)/418 (ash)
0.37	7 (sulfate/ash)	418 (sulfate)/625 (ash)

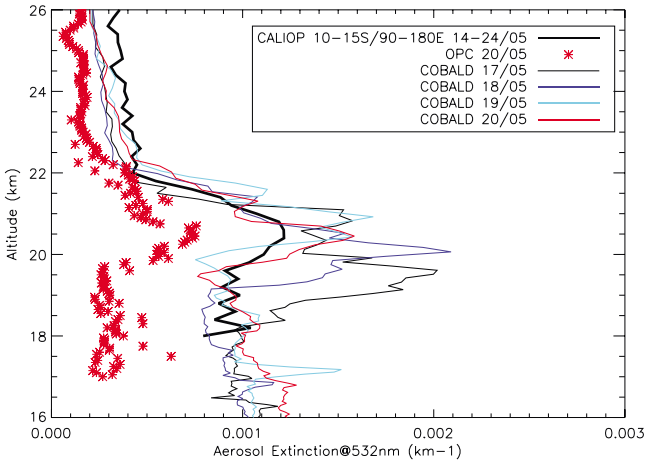

Figure 8. Extinction profiles derived from the following: (i) COBALD on 17–20 and 22 May, (ii) OPC on 20 May, and (ii) CALIOP averaged between 90 and 180°E, 10 and 15°S between 14 and 24 May.

tropics if acted on by the BD circulation, while it would descend three times faster without upward motions. Thus, fine volcanic ash in the tropical lower stratosphere can potentially persist for several months with subsequent radiative and climate impacts.

5. The Presence of Ash in the Kelud Plume

The volatility measurements during the KIAsh campaign showed the presence of solid ash particles in the bottom of the Kelud plume with radius $> 0.26\,\mu m$ and $> 0.37\,\mu m$ and a concentration between 20 and 60 particles/L. We compare aerosol extinction profiles derived from in situ COBALD and OPC measurements together with CALIOP in Figure 8. The COBALD SR at 532 nm is calculated using an Angstrom coefficient derived from the measurements at 455 nm and 940 nm as described in *Vernier et al.* [2015]. A standard molecular backscatter ($\beta_{m,r}$) at 1000 hPa and 273 K is calculated (equation (12)) by dividing a referenced molecular extinction (Ext = 0.013705 km^{-1} sr^{-1}) from *Bucholtz* [1995] with the molecular Lidar ratio ($L_m = 8\pi/3$).

The aerosol backscatter ratio (SR − 1) from COBALD is then multiplied by the referenced molecular density to obtain an aerosol backscatter coefficient, which is converted (equation (13)) into an aerosol extinction using a lidar ratio ($L_a = 45sr+/-10$). L_a is calculated by averaging the ash and sulfate lidar ratios of 40 sr and 50 sr used to convert CALIOP data in section 2.1

$$\beta_{m,r} = \frac{\alpha_{m,r}}{L_m} \tag{12}$$

$$\alpha_a = L_a \times \beta_{m,r} \times (SR - 1) \tag{13}$$

CALIOP total aerosol extinction is then calculated by adding the ash and sulfate extinction (see section 2.1).

The OPC and COBALD sensors were included under the same balloon flight on 20 May. We used bimodal and unimodal size distributions to fit the OPC measurements below and above 22 km, respectively. We calculate the aerosol extinction coefficient using the size distributions from the OPC flights and refractive index for sulfate and ash of 1.47 and 1.60 + 0.002*i* [*Ball et al.*, 2015], respectively, using Mie theory. Using an imaginary part of 0.0002, the lower bound estimated by *Ball et al.* [2015] leads to a decrease of aerosol extinction by a few percent only. We recognize that *T* matrix would represent an improvement over Mie theory for optical calculations involving nonspherical particles, and this impact will be explored in the future.

The plume was transported over Darwin during the campaign with a large variability in aerosol extinction below 20 km. For example, the aerosol extinction near 19 km is shown to be 2–3 times higher during the first two balloon flights compared to the last two (Figure 7).

The shapes of the OPC and COBALD profiles on May 20th are very similar, even in the fine structure, but differ in absolute values. The reasons for this discrepancy are under investigation but remain inconclusive at this time. The CALIOP extinction profile, calculated by averaging data between 13 and23 May and 10–15°S; 90–180°E, lies at the lower bounds of the COBALD profiles below 22 km.

We calculated the AOD between 18 and 23 km from these extinction profiles (see Table 2). We find a mean AOD from CALIOP near 0.0044, 4 to 25% below the values (0.0046–0.0055) derived from the COBALD flights but around twice the OPC result (0.0020). The ash fraction of the total AOD derived from CALIOP and OPC is near 10–11%. After removing the stratospheric sulfate background, we found that the contribution of the ash component increases up to 20 and 25% for OPC and CALIOP, respectively.

Table 2. AOD at 532 nm Between 18 and 23 km Calculated From CALIOP, COBALD, and OPC

Sensors AODs18–23 km	Total AOD	Total AODKelud	Ash AOD	Sulfate AOD	Sulfate AODKelud	Ash Fraction	Ash FractionKelud
CALIOP (10–15°S)	0.0044	0.0020	0.0005	0.0039	0.0014	11%	25%
COBALD17	0.0055	0.0025					
COBALD18	0.0049	0.0021					
COBALD19	0.0048	0.0014					
COBALD20	0.0046	0.0012					
OPC	0.0020	0.0010	0.0002	0.0018	0.0010	10%	20%

6. Radiative Forcings of the Kelud Plume

The radiative impact from the Kelud plume is examined using CALIPSO, in situ measurements collected during the KlAsh campaign, and a stand-alone radiative transfer model. By accumulating ash and sulfate extinction profiles derived from CALIPSO between 18 and 25 km for every 10 day period between 20°N–20°S during the first 3 months after the Kelud eruption, we calculated the zonal mean AOD and separated the contributions of ash and sulfate. The background sulfate aerosol corresponding to an aerosol extinction of near 0.0005 (Figure 4) is removed by subtracting the mean extinction calculated over 180°W–0° longitude where the plume was not transported during the first 10 days after the Kelud eruption. We found no apparent background in the ash extinction profiles over the same area (not shown) so that no ash background was removed. Figure 9 shows the mean ash and sulfate AOD with and without including the stratospheric sulfate background. The ash AOD is seen to decrease soon after the Kelud eruption and reaches nearly 0.001 after 3 months while the Kelud-sulfate (no background) AOD at 532 nm increases up to 50–60 days after the eruption before remaining at a relatively constant level near 0.0025–0.003. At the end of the period, the ash AOD contributes nearly 28% of the total AOD after removing the stratospheric sulfate background and to 15% with the background aerosol. Using OPC and CALIOP data, we can then estimate that the ash component of the plume is within 20 to 28% of the total AOD more than 3 months after the eruption.

We calculated the radiative forcing (RF) at the top of the atmosphere from the Kelud plume using a stand-alone radiative transfer model [*Natarajan et al.*, 2012] for the first 3 months after the eruption. The model includes aerosol effects due to short-wave (SW) and long-wave (LW) scattering and absorption, and emission (LW). Background distributions of pressure, temperature, water vapor, ozone, cloud optical depth, and cloud fraction profiles were adopted from the Global Modeling Initiative (GMI) model simulations with metfields from Modern Era Retrospective analysis for Research and Applications analyses. The radiative transfer model makes use of vertical profiles of aerosol extinction due to sulfate and ash obtained from the CALIOP satellite data. The input optical properties of aerosols, which include extinction efficiency, single scattering albedo, and asymmetry factors, were evaluated using the bimodal distributions of sulfate and ash particles derived from the OPC data obtained during the KlAsh campaign. For volcanic sulfate droplets, the radius and the standard deviation for the first mode are 0.1 μm and 1.25. For the second mode, they are 0.25 μm and 1.4. In the case of volcanic ash particles, the radius is 0.05 μm for the first mode and 0.25 μm for the second mode. The standard deviation is 1.4 for both the modes.

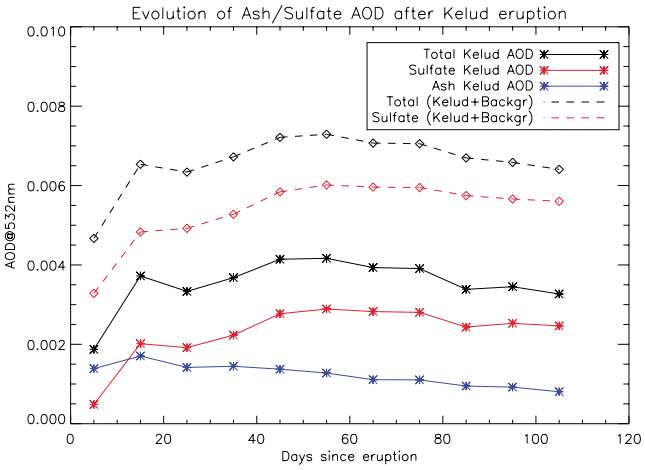

Figure 9. The 10 day period zonal mean (20°N–20°S) AODs calculated between 18 and 25 km during the first 3 months after the Kelud eruption.

Table 3 shows SW and LW RF at the top of the atmosphere (TOA) and RF per unit AOD from radiative model calculation conducted using the AOD profile for 14 March 2014 shown in Figure 2b. The aerosol optical properties are based on the bimodal distributions for sulfate and ash obtained during the KlAsh

Table 3. TOA Radiative Effects Due To Kelud Volcanic Aerosol at 140°W and Equator[a]

Aerosol Type	AOD	TOAΔSW (W/m^2)	TOAΔLW (W/m^2)	TOARF (W/m^2)	RF Per Unit AOD (W/m^2)
Sulfate	0.0078	−0.348	−0.149	−0.199	−25.5
Ash	0.0045	−0.180	−0.035	−0.145	−32.2
Sulfate + ash	0.0123	−0.527	−0.184	−0.343	−27.9

[a]The aerosol extinction profiles used in the radiative calculations correspond to the CALIPSO data for 14 March 2014. Microphysical properties of ash and sulfate are derived from the KIAsh campaign.

balloon campaign. The mean RF efficiency of sulfate aerosol alone is near −25 W/m^2 for each unit of AOD, while that of fine ash particles is 30% larger. Knowing the fraction of ash and sulfate in a volcanic plume is important to correctly compute its radiative impact.

Figure 10 shows the RF at the TOA for clear sky assuming that the plume contains externally mixed sulfate and ash particles and using derived ash and sulfate extinction coefficients from CALIOP and size information from OPC. Three months after the eruption (beginning of June), the clear-sky RF values including ash are 20–25% larger (near −0.08 W/m^2) than the sulfate case only. Thus, we show that neglecting the radiative impact of volcanic ash can underestimate the overall volcanic RF from the Kelud eruption and consequently the surface cooling from this eruption.

7. Discussion

Ash particles in volcanic plumes have often been considered to have a negligible effect on climate due to their much shorter lifetime compared to sulfate aerosol due to their removal by sedimentation and scavenging. *Niemeier et al.* [2009] used the MAECHAM5 model to simulate the dispersal of the volcanic plume from the 1991 Mount Pinatubo eruption. They found an ash lifetime in the Pinatubo volcanic plume of only a few days, concluding that ash particles had a minor impact in climate. Most globally and vertically resolved observations of Mount Pinatubo volcanic plume have relied on solar occultation measurements (Stratospheric Aerosol and Gas Experiment and Halogen Occultation Experiment) from which distinguishing ash and sulfate is challenging. Aircraft lidar observations in the Caribbean have shown the presence of depolarizing layers near 23 km 1 month after Mount Pinatubo eruption [*Winker and Osborn*, 1992]. In situ observations at 41°N showed nonvolatile ash layers at 18 and 23 km at 40 and 44 days after the Pinatubo eruption [*Deshler et al.*, 1992] and electron microscope analysis indicated the presence of crustal particles [*Sheridan et al.*, 1992]. Japanese ground-based lidars have also monitored the depolarization coefficient within the Mount Pinatubo and El Chichón plumes, finding that ash lasted for several months in those plumes [*Hayashida et al.*, 1984; *Nagai et al.*, 1993]. These all indicate a longer lifetime for ash in volcanic eruptions than is frequently assumed. Figure 11 shows the PDFs of the particulate depolarization ratio, used as a proxy for the presence of ash, observed by CALIOP during the first 30 days following the Kasatochi, Sarychev, Pueyhue-Cordon and Kelud eruptions, at different altitude and latitude bands. The Pueyhue-Cordon was largely composed of ash particles with the mode of depolarization ~0.36 approaching values observed (0.39) for mineral dust [*Vernier et al.*, 2013; *Sakai et al.*, 2010]. On the other hand, the Sarychev plume was

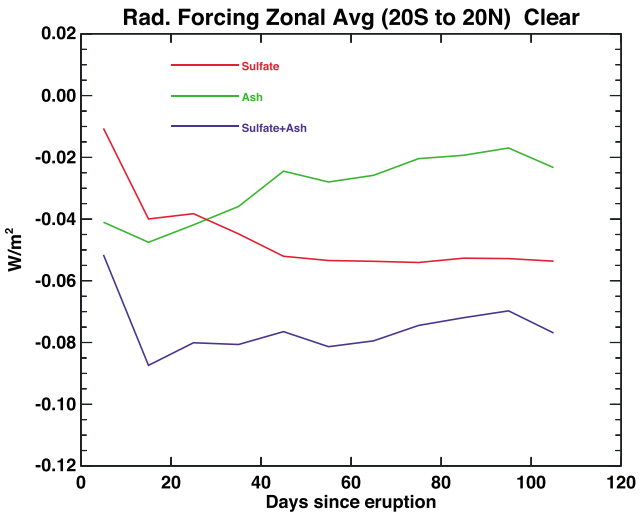

Figure 10. Zonal clear-sky top of the atmosphere radiative forcing between 20°N and 20°S calculated after the Kelud eruption for sulfate aerosol only (red), ash (green), and sulfate + ash (blue).

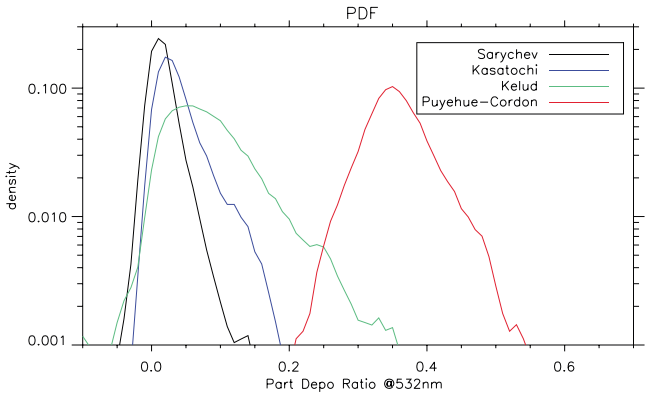

Figure 11. Probability density functions of the particulate depolarization ratio from CALIOP observations of volcanic plumes during the first 30 days following each eruption (Kasatochi: 08/07/2008, 50–60°N, 16–19 km; Sarychev: 06/12/2009, 50–60°N, 16–19 km; Puyehue-Cordon: 06/04/2011; 50–60°S, 9–13 km; Kelud: 02/13/2014, 20°S–20°N, 19.5–20.5 km).

largely composed of sulfate aerosol as shown by the mode of its PDF near 0.01, consistent with the presence of spherical particles. With a distribution skewed toward higher depolarization values, we showed in this paper that the Kelud plume was composed of a mixture of ash and sulfate. CALIPSO observations of several volcanic plumes during the past decade show that plume composition can vary considerably depending on the initial injection of ultrafine ash and SO_2 further oxidized into sulfate. It is too simple to assume that volcanic plumes are made entirely of sulfate, even several months after an eruption. Another factor playing an important role on the lifetime of ash is the latitude of the eruption. Indeed, ash injected in the tropics has a longer lifetime because of the upward motion associated with the Brewer-Dobson circulation. A summary of volcanic ash observations shown in Table 2 demonstrates that it is appropriate to consider the climate impacts of volcanic ash following certain types of eruption and should improve our understanding of the climate impacts of volcanoes.

8. Conclusions

We have shown that depolarization measurements from CALIPSO provide an effective method to distinguish aspherical (e.g., ash) particles from spherical particles (e.g., sulfate) and have used this technique to diagnose the AOD contributions from ash and sulfate in the Kelud plume, as seen by CALIPSO. We find that 3 months after the eruption, 20–25% of total Kelud AOD between 18 and 23 km comes from the presence of ash. The persistence of a fine mode of ash particles in the lower part of the Kelud volcanic cloud is confirmed through in situ OPC measurements of ash particles with a radius near 0.3 μm made during the KlAsh campaign to northern Australia in May 2014.

Table 4. Eruption's Name and Volcanic Ash Observations

Volcano	References	Lifetime of Ash
Agung, 1963	*Mossop* [1964]	Volcanic ash sampled at 20 km by aircraft up to 1 year after the eruption (ash radius decrease from 0.4 to 0.2 μm)
Mount St. Helens, 1980	*Turco et al.* [1983], *Oberbeck et al.* [1983]	Volcanic ash coated with sulfate of 0.1–3 μm observed a month after the eruption; ground-based measurements of high depolarization (presence of ash) several months after the eruption in Hampton, VA, USA
El Chichón, 1982	*Hayashida et al.* [1984]	Depolarizing layers observed over Japan up to 5–6 months after the eruption
Mount Pinatubo, 1991	*Winker and Osborn* [1992], *Nagai et al.* [1993], *Pueschel et al.* [1994], *Deshler et al.* [1992], and *Sheridan et al.* [1992]	Depolarizing layers at 23 km in the Caribbean 26 days after the eruption by aircraft and near 18–20 km up to 8 months observed with ground-based lidar in Japan; nonvolatile layers at 18 and 23 km 40–44 days after the eruption by balloon-borne in situ measurements; electron microscope analysis of crustal particles
Puyehue-Cordon, 2011	*Vernier et al.* [2013]	Depolarizing layers (0.3–0.4) observed several weeks in the Southern Hemisphere after the eruption near 12–13 km
Mount Kelud, 2014	This study	Light depolarization observed by CALIPSO and ash particles sampled by balloon-borne OPC at the bottom of the plume 3 months after the eruption

Through in situ and global observations made in the Kelud volcanic plume and a number of published but rarely cited studies (Table 4) following major volcanic eruptions, we show in this paper that the radiative impact of ash is significant, in particular fortropical eruptions, where the Brewer Dobson circulation can sustain small ash in the stratosphere longer than generally assumed. We estimate a clear sky tropical RF of -0.07 to -0.08 W/m^2 up to 3 months after the Kelud volcanic eruption, including the presence of ash particles. RF estimates are similar to those observed after medium volcanic eruptions over the past decade [*Solomon et al*., 2011; *Santer et al*., 2014; *Andersson et al*., 2015], leading to a small temporary surface temperature cooling.

Acknowledgments
We would like to thank D. Considine and J. Kay (NASA HQ), the CALIPSO, and SAGE groups for supporting the KlAsh deployment in Australia. We also thank B. Atkinson and others at the Bureau of Meteorology in Darwin for logistical support during the campaign. We would like to thank Kam-Pui Lee for helping to produce Figures 2a and 2b. We would like to thank the Civil Aviation Safety Authority in Australia and local air traffic services in Darwin. The CALIPSO data can be obtained through the Atmospheric Data Center at NASA Langley (https://eosweb.larc.nasa.gov/project/calipso/calipso_table). The data collected during the KlAsh campaign can be obtained through correspondence with Jean-Paul Vernier (jeanpaul.vernier@nasa.gov).

References

Andersson, M. S., B. G. Martinsson, J.-P. Vernier, J. Friberg, C. A. M. Brenninkmeijer, M. Hermann, P. F. J. van Velthoven, and A. Zahn (2015), Significant radiative impact of volcanic aerosol in the lowermost stratosphere, *Nat. Commun.*, *6*, 7692, doi:10.1038/ncomms8692.

Ansmann, A., et al. (2010), The 16 April 2010 major volcanic ash plume over central Europe: EARLINET lidar and AERONET photometer observations at Leipzig and Munich, Germany, *Geophys. Res. Lett.*, *37*, L13810, doi:10.1029/2010GL043809.

Ansmann, A., et al. (2011), Ash and fine-mode particle mass profiles from EARLINET-AERONET observations over central Europe after the eruptions of the Eyjafjallajökull volcano in 2010, *J. Geophys. Res.*, *116*, D00U02, doi:10.1029/2010JD015567.

Ball, J. G. C., B. E. Reed, R. G. Grainger, D. M. Peters, T. A. Mather, and D. M. Pyle (2015), Measurements of the complex refractive index of volcanic ash at 450, 546.7, and 650 nm, *J. Geophys. Res. Atmos.*, *120*, 7747–7757, doi:10.1002/2015JD023521.

Brabec, M., F. G. Wienhold, B. P. Luo, H. Vömel, F. Immler, P. Steiner, E. Hausammann, U. Weers, and T. Peter (2012), Particle backscatter and relative humidity measured across cirrus clouds and comparison with microphysical cirrus modeling, *Atmos. Chem. Phys.*, *12*, 9135–9148, doi:10.5194/acp-12-9135-2012.

Browell, E. V., C. F. Butler, M. A. Fenn, W. B. Grant, S. Ismail, M. Schoeberl, O. B. Toon, M. Loewenstein, and J. Podolske (1993), Ozone and aerosol changes observed during the 1991–92 Airborne Arctic Stratospheric Expedition, *Science*, *261*, 1155–1158.

Bucholtz, A. (1995), Rayleigh-scattering calculations for the terrestrial atmosphere, *Appl. Opt.*, *34*, 2765–2773.

Cairo, F., G. Di Donfrancesco, A. Adriani, L. Pulvirenti, and F. Fierli (1999), Comparison of various linear depolarization parameters measured by lidar, *Appl. Opt.*, *38*, 4425–4432, doi:10.1364/AO.38.004425.

Campbell, P., and T. Deshler (2014), Condensation nuclei measurements in the midlatitude (1982–2012) and Antarctic (1986–2010) stratosphere between 20 and 35 km, *J. Geophys. Res. Atmos.*, *119*, 137–152, doi:10.1002/2013JD019710.

Carn, S. A., and F. J. Prata (2010), Satellite-based constraints on explosive SO_2 release from Soufrière Hills Volcano, Montserrat, *Geophys. Res. Lett.*, *37*, L00E22, doi:10.1029/2010GL044971.

Clarisse, L., P.-F. Coheur, N. Theys, D. Hurtmans, and C. Clerbaux (2014), The 2011 Nabro eruption, a SO_2 plume height analysis using IASI measurements, *Atmos. Chem. Phys.*, *14*, 3095–3111, doi:10.5194/acp-14-3095-2014.

Corti, T., B. P. Luo, P. Peter, H. Vömel, and Q. Fu (2005), Mean radiative energy balance and vertical mass fluxes in the equatorial upper troposphere and lower stratosphere, *Geophys. Res. Lett.*, *32*, L06802, doi:10.1029/2004GL021889.

Deshler, T., D. J. Hofmann, B. J. Johnson, and W. R. Rozier (1992), Balloonborne measurements of the Pinatubo aerosol size distribution and volatility at Laramie, Wyoming during the summer of 1991, *Geophys. Res. Lett.*, *19*, 199–202, doi:10.1029/91GL02787.

Deshler, T., M. E. Hervig, D. J. Hofmann, J. M. Rosen, and J. B. Liley (2003), Thirty years of in situ stratospheric aerosol size distribution measurements from Laramie, Wyoming (41°N), using balloon-borne instruments, *J. Geophys. Res.*, *108*(D5), 4167, doi:10.1029/2002JD002514.

Fyfe, J. C., K. von Salzen, J. N. S. Cole, N. P. Gillett, and J.-P. Vernier (2013), Surface response to stratospheric aerosol changes in a coupled atmosphere-ocean model, *Geophys. Res. Lett.*, *40*, 584–588, doi:10.1002/grl.50156.

Groß, S., J. Gasteiger, V. Freudenthaler, F. Schnell, and M. Wiegner (2010), Characterization of the Eyjafjallajökull ash-plume by means of lidar measurements over the Munich EARLINET site, *Proc. SPIE*, *7832*, doi:10.1117/12.869020.

Hamill, P., E. J. Jensen, P. B. Russell, and J. J. Bauman (1997), The life cycle of stratospheric aerosol particles, *Bull. Am. Meteorol. Soc.*, *78*, 1395–1410.

Hansen, J., A. Lacis, R. Ruedy, and M. Sato (1992), Potential climate impact of Mount Pinatubo eruption, *Geophys. Res. Lett.*, *19*, 215–218, doi:10.1029/91GL02788.

Hansen, J., et al. (2005), Efficacy of climate forcings, *J. Geophys. Res.*, *110*, D18104, doi:10.1029/2005JD005776.

Hayashida, S., and Y. Sasano (1993), Stratospheric aerosol change in the early stage of volcanic disturbance by the Pinatubo eruption observed over Tsukuba, Japan, *Geophys. Res. Lett.*, *20*, 575–578, doi:10.1029/93GL00511.

Hayashida, S., A. Kobayashi, and Y. Iwasaka (1984), Lidar measurements of stratospheric aerosol content and depolarization ratio after the eruption of volcano E1 Chichon: Measurements at Nagoya, *Japan. Geof. Int.*, *23*, 277–288.

Hobbs, P. V., L. F. Radke, J. H. Lyons, R. J. Federek, D. J. Coffman, and T. J. Casadevall (1991), Airborne measurements of particle and gas emissions from the 1990 volcanic eruptions of Mount Redoubt, *J. Geophys. Res.*, *96*, 18,735–18,752, doi:10.1029/91JD01635.

Jager, H., and T. Deshler (2002), Lidar backscatter to extinction, mass and area conversions for stratospheric aerosols based on midlatitude balloonborne size distribution measurements, *Geophys. Res. Lett.*, *29*(19), 1929, doi:10.1029/2002GL015609.

Jager, H., and T. Deshler (2003), Correction to lidar backscatter to extinction, mass and area conversions for stratospheric aerosols based on midlatitude balloonborne size distribution measurements, *Geophys. Res. Lett.*, *30*(7), 1382, doi:10.1029/2003GL017189.

Kristiansen, N. I., A. J. Prata, A. Stohl, and S. A. Carn (2015), Stratospheric volcanic ash emissions from the 13 February 2014 Kelut eruption, *Geophys. Res. Lett.*, *42*, 588–596, doi:10.1002/2014GL062307.

Mattis, I., P. Seifert, D. Müller, M. Tesche, A. Hiebsch, T. Kanitz, J. Schmidt, F. Finger, U. Wandinger, and A. Ansmann (2010), Volcanic aerosol layers observed with multiwavelength Raman lidar over central Europe in 2008–2009, *J. Geophys. Res.*, *115*, D00L04, doi:10.1029/2009JD013472.

Mossop, S. C. (1964), Volcanic dust collected at an altitude of 20 KM, *Nature*, *203*, 824–827, doi:10.1038/203824a0.

Nagai, T., O. Uchino, T. Fujimoto, Y. Sai, K. Tamashiro, R. Nomura, and T. Sunagawa (1993), Lidar observation of the stratospheric aerosol layer over Okinawa, Japan, after the Mt. Pinatubo volcanic eruption, *J. Meteor. Soc. Jpn.*, *71*, 749–755.

Natarajan, M., R. B. Pierce, T. K. Schaack, A. J. Lenzen, J. A. Al-Saadi, A. J. Soja, T. P. Charlock, F. G. Rose, D. M. Winker, and J. R. Worden (2012), Radiative forcing due to enhancements in tropospheric ozone and carbonaceous aerosols caused by Asian fires during spring 2008, *J. Geophys. Res.*, *117*, D06307, doi:10.1029/2011JD016584.

Niemeier, U., C. Timmreck, H.-F. Graf, S. Kinne, S. Rast, and S. Self (2009), Initial fate of fine ash and sulfur from large volcanic eruptions, *Atmos. Chem. Phys.*, *9*, 9043–9057, doi:10.5194/acp-9-9043-2009.

Oberbeck, V. R., E. F. Danielsen, K. G. Snetsinger, G. V. Ferry, W. Fong, and D. M. Hayes (1983), Effect of the eruption of El Chichon on stratospheric aerosol size and composition, *Geophys. Res. Lett.*, *10*, 1021–1024, doi:10.1029/GL010i011p01021.

Pueschel, R. F., J. M. Livingston, P. B. Russell, and S. Verma (1994),Physical and optical properties of the Pinatubo volcanic aerosol: Aircraft observations with impactors and a suntracking photometer, *J. Geophys. Res.*, *95*, 12,915–12,922.

Pueschel, R., P. B. Russell, D. A. Allen, G. V. Ferry, K. G. Snetsinger, J. M. Livingston, and S. Verma (1994), Physical and optical properties of the Pinatubo volcanic aerosol: Aircrafts with impactors and a Suntracking photometer, *J. Geophys. Res.*, *99*, 12,915–12,922, doi:10.1029/94JD00621.

Robock, A. (2000), Volcanic eruptions and climate, *Rev. Geophys.*, *38*, 191–219, doi:10.1029/1998RG000054.

Rosenlof, K. H. (1995), Seasonal cycle of the residual mean meridional circulation in the stratosphere, *J. Geophys. Res.*, *100*, 5173–5191, doi:10.1029/94JD03122.

Sakai, T., T. Nagai, Y. Zaizen, and Y. Mano (2010), Backscattering linear depolarization ratio measurements of mineral, sea-salt, and ammonium sulfate particles simulated in a laboratory chamber, *Appl. Optics*, *49*, 4441–4449.

Santer, B. D., et al. (2014), Volcanic contribution to decadal changes in tropospheric temperature, *Nat. Geosci.*, *7*(3), 185–189, doi:10.1038/ngeo2098.

Schumann, U., et al. (2011), Airborne observations of the Eyjafjalla volcano ash cloud over Europe during air space closure in April and May 2010, *Atmos. Chem. Phys.*, *11*, 2245–2279.

Sheridan, P. J., R. C. Schnell, D. J. Hofmann, and T. Deshler (1992), Electron microscope studies of Mt. Pinatubo aerosol layers over Laramie, Wyoming, during summer 1991, *Geophys. Res. Lett.*, *19*, 203–206, doi:10.1029/91GL02789.

Solomon, S., J. S. Daniel, R. R. Neely III, J.-P. Vernier, E. G. Dutton, and L. W. Thomason (2011), The persistently variable "background" stratospheric aerosol layer and global climate change, *Science*, *333*(6044), 866–870, doi:10.1126/science.1206027.

Sugimoto, N., and C. H. Lee (2006), Characteristics of dust aerosols inferred from lidar depolarization measurements at two wavelengths, *Appl. Opt.*, *45*, 7468–7474.

Tesche, M., A. Ansmann, D. Müller, D. Althausen, R. Engelmann, V. Freudenthaler, and S. Groß (2009), Vertically resolved separation of dust and smoke over Cape Verde using multiwavelength Raman and polarization lidars during Saharan Mineral Dust Experiment 2008, *J. Geophys. Res.*, *114*, D13202, doi:10.1029/2009JD011862.

Trepte, C. R., and M. H. Hitchman (1992), Tropical stratospheric circulation deduced from satellite aerosol data, *Nature*, *355*, 626–628.

Turco, R. P., O. B. Toon, R. C. Whitten, P. Hamill, and R. G. Keesee (1983), The 1980 eruptions of Mount St. Helens: Physical and chemical processes in the stratospheric clouds, *J. Geophys. Res.*, *88*(C9), 5299–5319, doi:10.1029/JC088iC09p05299.

Vernier, J.-P., et al. (2009), Tropical stratospheric aerosol layer from CALIPSO lidar observations, *J. Geophys. Res.*, *114*, D00H10, doi:10.1029/2009JD011946.

Vernier, J.-P., et al. (2011), Major influence of tropical volcanic eruptions on the stratospheric aerosol layer during the last decade, *Geophys. Res. Lett.*, *38*, L12807, doi:10.1029/2011GL047563.

Vernier, J.-P., et al. (2013), Monitoring the 3D structure of diffuse volcanic ash clouds, *J. Appl. Meteorol. Climatol.*, *52*, 2125–2138, doi:10.1175/JAMC-D-12-0279.1.

Vernier, J.-P., T. D. Fairlie, M. Natarajan, F. G. Wienhold, J. Bian, B. G. Martinsson, S. Crumeyrolle, L. W. Thomason, and K. K. Bedka (2015), Increase in upper tropospheric and lower stratospheric aerosol levels and its potential connection with Asian pollution, *J. Geophys. Res. Atmos.*, *120*, 1608–1619, doi:10.1002/2014JD022372.

Winker, D. M., and M. T. Osborn (1992), Airborne lidar observations of the Pinatubo volcanic plume, *Geophys. Res. Lett.*, *19*, 167–170, doi:10.1029/91GL02867.

Winker, D. M., et al. (2010), The CALIPSO Mission: A global 3D view of aerosol and clouds, *Bull. Am. Meteorol. Soc.*, *91*(9), 1211–1229, doi:10.1175/2010BAMS3009.1.

Winker, D. M., Z. Liu, A. Omar, J. Tackett, and D. Fairlie (2012), CALIOP observations of the transport of ash from the Eyjafjallajökull volcano in April 2010, *J. Geophys. Res.*, *117*, D00U15, doi:10.1029/2011JD016499.